A VQ-Based Approach to Thermal Image Analysis for Printed Circuit Boards Diagnosis

Shih-Yuan Huang, Chi-Wu Mao, and Kuo-Sheng Cheng, *Senior Member, IEEE*

***Abstract*—This paper proposes a novel method to analyze the thermal image of a printed circuit board (PCB) for fault detection. In this method, a gold thermal image is first generated from the thermal images of the PCB in normal operation, and then compressed into a codebook with a certain number of codewords. Each codeword represents a block of image size four by four. Each block in the thermal image for the board under test (BUT) is then encoded in the same way. The codewords in the codebook are arranged in ascending order with respect to their mean values. Any abnormal functional block in BUT can be identified by comparing the codeword index with that of the corresponding block in the gold thermal image. The memory size for storing the templates for comparison is, thus, significantly reduced without diagnosis performance degradation. Also, there is not a necessity for feature extraction such as the feature-based diagnostic methods. In addition, an adaptive threshold criterion is proposed to improve the detection sensitivity. From the experimental results, this proposed method is demonstrated to be very effective in abnormal functional block identification for PCBs based on the thermal image. Furthermore, this method is highly modularized for hardware implementation and parallel realization to speed up the processing time.**

***Index Terms*—Hopfield neural network, printed circuit board (PCB), thermal image, vector quantization.**

I. Introduction

THE conventional automatic test equipment (ATE) has some limitations and drawbacks. To name a few, a large paradox group may result in poor fault isolation, the complexity of printed circuit board (PCB) can cause many difficulties in testing, the irregular faults may lead to improper or incomplete diagnosis, the electronic component interaction may interfere with the data measurements in probing, and so on [1]. Accordingly, several nondestructive diagnostic techniques have been developed to facilitate the ATE. These include optical imaging, X-ray imaging, magnetic field mapping, and thermal imaging approaches [2]. Among all the methods, the thermal image of PCB can significantly reveal the faults such as the broken internal connection, short-circuit loop, open-circuit node, power supply failure, signal interaction, and component malfunction. In addition, the thermal imaging diagnostic system has the advantages of no contact problem, rapid image acquisition, easy operation, and simple testing reconfiguration. Therefore, the thermal imaging approach has been widely applied in the past decade to diagnose faults on PCBs [1]–[15].

Among these techniques, the artificial neural network-based approach is widely used. In this approach, the diagnostic rules/relationships are first developed for training the neural networks in a supervised or unsupervised way with the thermal features and known faults. The generally used thermal features include peak temperature, mean temperature, maximal temperature gradient, and temperature difference measures [1], [10]. Second, the segmentation of the thermal image is required to find out the abnormal hot/cold spots and identify the most likely failure sites with the highest probability of occurrence based on some distribution, especially the F distribution [6], [12], [13]. Finally, the thermal image data is acquired from the designed system setup and fed to the neural network for fault diagnosis and identification [9].

In the thermal image processing mentioned above, the well-known "gold thermal image" has been used in all methods. The thermal features defined for the gold thermal image include the rate of temperature change, peak temperature, averaged temperature, and hot spots. In this paper, the peak temperature is used as the thermal feature for our application. In the traditional algorithm, one gold thermal image contains one feature only. The more the features used, the more the memory size that will be needed. The thermal image for the printed circuit board under test is then compared with these gold thermal images in sequence. Therefore, how to reduce the memory size for storing the gold thermal images and how to concurrently process the gold thermal image become the interesting issues in PCB analysis.

In this paper, a novel vector quantization (VQ)-based approach that not only reduces the memory size but also compares each codeword is proposed. The gold thermal image is coded into a codebook and compared with the BUT to identify the image blocks with faults, instead of the whole thermal image. VQ is a popular and effective method used for image compression. It has the merit of keeping the major feature of an image during the codebook generation with only a minimal distortion. Thus, the memory size for the gold thermal image may be significantly reduced. As long as the VQ algorithm provides high signal-to-noise ratio, the distortion of the gold thermal image can be minimized. In addition, a new adaptive threshold criterion is also proposed here for improving the sensitivity.

The remainder of this paper is organized as follows. Section II describes the proposed methods in detail. Section III gives several application examples with results, and finally the concluding remarks are made in Section IV.

Manuscript received August 14, 2003; revised March 19, 2005. This work was supported in part by the National Science Council, R.O.C. under Grant NSC 89-2213-E-006-095.

S.-Y. Huang and C.-W. Mao are with the Department of Electrical Engineering, National Cheng Kung University, Tainan 701, Taiwan, R.O.C.

K.-S. Cheng is with the Institute of Biomedical Engineering, National Cheng Kung University, Tainan 701, Taiwan, R.O.C. (e-mail: kscheng@mail.ncku.edu.tw).

Digital Object Identifier 10.1109/TIM.2005.858546

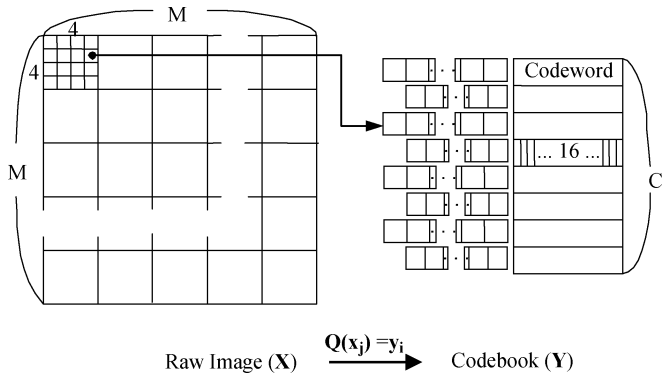

Fig. 1. Thermal image represented by codeword using vector quantization.

II. VQ-Based Thermal Image Analysis

For the sake of completeness, the basics of the temperature and thermal radiation are briefly summarized in the following. Any object with the temperature above 0 K will radiate thermal energy over all wavelengths which may be described as [16], [17]

$$W(T) = \sigma T^4 \tag{1}$$

where σ denotes the Stefan–Boltzmann constant $(5.670 \times 10^{-8}\ \mathrm{W/m^2K^4})$, and T is absolute temperature K. In practice, no objects would radiate the thermal energy as the ideal blackbody does. Thus, (1) should be modified to

$$W(T) = \varepsilon \sigma T^4 \tag{2}$$

where ε is the emissivity of the object $(0 < \varepsilon < 1)$. In this experiment, the emissivity for the same type of printed circuit board is assumed to be constant and may be neglected in the fault diagnosis. In other words, only the relative temperature changes between BUT and the gold thermal image are used for PCB function diagnosis.

A. Compensated Fuzzy Hopfield Neural Network for Vector Quantization

VQ is a widely applied and very efficient method to low-bit-rate image compression [18] and several algorithms have been proposed in the past two decades [18]–[22]. In this paper, VQ is employed to generate a codebook such that the image is approximated by the associated codewords with a minimal distortion. Basically, VQ may be defined as a mapping from a $l \times l$-dimensional Euclidean space $R^{l \times l}$ to a finite subset of $R^{l \times l}$ as illustrated in Fig. 1. The important points in the VQ-based codebook generation are how and with what to train its vectors. Here, clustering process is considered, in which the training vectors are classified into their attributed classes based on the minimization of average distortion between the training vector and the codewords.

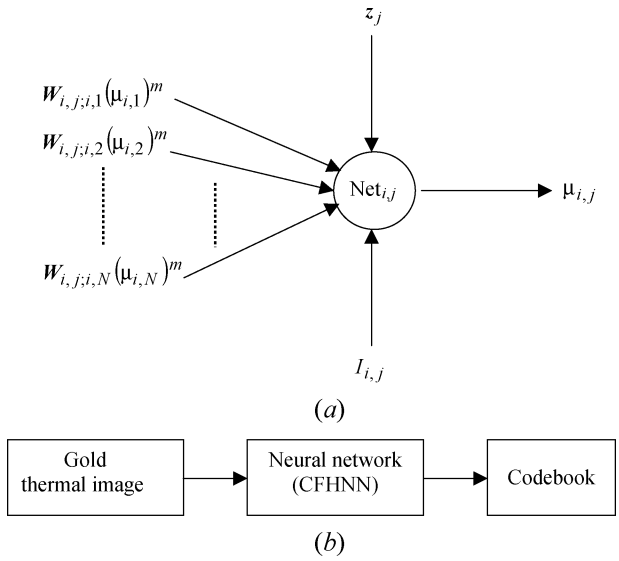

Fig. 2. (a) Signal-flow graph for $\mu_{i,j}$ in the CFHNN. (b) The block diagram of the codebook design phase.

An often-used method to assess the quality of image reconstructed from the codebook is the peak signal to noise ratio (PSNR). For an $N \times N$ image, it may be defined as follows:

$$\mathrm{PSNR} = 10 \log_{10} \frac{255 \times 255}{\frac{1}{N^2} \sum_{i=1}^{N} \sum_{j=1}^{N} (f_{i,j} - \hat{f}_{i,j})^2} \tag{3}$$

where $f_{i,j}$ and $\hat{f}_{i,j}$ are the gray levels of pixel (i, j) for the original and reconstructed images, respectively. Two hundred fifty five is the peak gray level.

In this paper, the compensated fuzzy Hopfield neural network (CFHNN) algorithm [22] is employed for codebook generation due to its features of fast convergence and easy energy computation. The CFHNN algorithm integrates the compensated fuzzy c-mean model into the learning scheme and updating strategy of the Hopfield neural network. The energy function is formulated on the basis of within-class scatter matrix. The within-class scatter matrix is defined to be the average distortion between the training vectors and the codewords within the same class. In [21], [22], a 256×256 real image was divided into 4×4 blocks to generate 4096 nonoverlapping 16-dimensional training vectors. Then, the codebook of size 64 was built using this training data. Lin *et al.* showed that a CFHNN algorithm can produce PSNR over 1.75 to 2.5 dB for image vector quantization of Lena, F-16, Girl, and Boy-girl images. It was also demonstrated to be better than the K-means and LBG (Linde Buzo Gray) algorithms [21].

Let $\mu_{i,j}$ represent the membership function for the training sample $\boldsymbol{z}_j$ associated with ith codeword $\boldsymbol{w}_i$. It is also the fuzzy output state of the (i, j) neuron. $\boldsymbol{W}_{i,j;i,k}$ is the interconnecting weight between neuron (i, j) and neuron (i, k), and $I_{i,j}$ the bias input of neuron (i, j). Fig. 2(a) shows the signal-flow graph

local to $\mu_{i,j}$. The total input to neuron (i,j) in Fig. 2(a) is computed as

$$Net_{i,j} = \left| \boldsymbol{z}_j - \sum_{k=1}^{N} \boldsymbol{W}_{i,j;i,k} (\mu_{i,k})^m \right|^2 + I_{i,j}. \quad (4)$$

$\sum_{k=1}^{N} \boldsymbol{W}_{i,j;i,k}$ in (4), is the total weighted input received from neuron (i,k) in column i, and m is the fuzzification parameter. In practice, an $l \times l$ block of training sample $\boldsymbol{z}_j$ is rearranged to a $1 \times L$ vector for $j = 1, 2, \ldots, N$. The dimension of $\boldsymbol{W}_{i,j;i,k}$ is $1 \times L$ and both $\mu_{i,j}$ and $I_{i,j}$ are scalars. Each column of this two-dimensional modified Hopfield network represents a class and each row represents a membership for the ith class. Let $\sum_{k=1}^{N} \boldsymbol{W}_{i,j;i,k} (\mu_{i,k})^m$ be the ith codeword $\boldsymbol{w}_i$ so that (4) involves the Euclidean distance between the training vector $\boldsymbol{z}_j$ and codeword $\boldsymbol{w}_i$. Consequently, the Lyapunov energy function of this network when using compensated fuzzy c-means (CFCM) strategy, is defined as

$$E = \frac{1}{2} \sum_{i=1}^{C} \sum_{j=1}^{N} (\mu_{i,j})^m Net_{i,j} \quad (5)$$

In order to embed CFCM into CFHNN, the interconnecting weight vector $W_{i,j;i,k}$ is computed as

$$\boldsymbol{W}_{i,j;i,k} = \frac{\boldsymbol{z}_k}{\sum_{k=1}^{N} (\mu_{i,k})^m}. \quad (6)$$

Furthermore, for speeding up the convergence rate of the energy function, the input bias $I_{i,j} = \nu \tanh(\alpha_i)$ proposed by Lin [22] is also used here. ν is a constant greater than zero and α_i is defined as

$$\alpha_i = \frac{\sum_{j=1}^{N} (\mu_{i,j})^m}{\sum_{i=1}^{C} \sum_{j=1}^{N} (\mu_{i,j})^m}; \quad i = 1, 2, \ldots, C. \quad (7)$$

Finally, the output state at neuron (i,j) is obtained as

$$\mu_{i,j} = \frac{(Net_{i,j})^{-\frac{1}{m-1}}}{\sum_{i=1}^{C} (Net_{i,j})^{-\frac{1}{m-1}}}. \quad (8)$$

The codebook generation is accomplished when the energy E in (5) converges to a minimum. The ith codeword $\boldsymbol{w}_i$ will be given as

$$\boldsymbol{w}_i = \sum_{k=1}^{N} \frac{\boldsymbol{z}_k (\mu_{i,k})^m}{\sum_{j=1}^{N} (\mu_{i,j})^m}, \quad i = 1, 2, \ldots, C. \quad (9)$$

B. Implementation

The gold thermal image is constructed by collecting the maximal operating temperatures of all normal thermal images. That is, the maximal temperature of every corresponding pixel for five normal thermal images is collected and recorded as the gold thermal image for comparison. Then this gold image is divided into 400 4×4 nonoverlapping blocks. In practice, the block of the training sample $\boldsymbol{z}_j$ is represented as a 1×16 vector for $j = 1, 2, \ldots, 400$. Then, the CFHNN is applied to generate a codebook containing 64 codewords (i.e., $L = 16$, $N = 400$, $C = 64$). While applying the CFHNN to design a codebook associated with the gold thermal image, almost all the thermal information is blended into this codebook. Consequently, in the encoding phase each block (i.e., training sample $\boldsymbol{z}_j$) of gold thermal image can be assigned to an index i in a sense of least square Euclidean distance between the training sample z_j and each codeword $\boldsymbol{w}_i$. However, many algorithms based on Euclidean distance and Cauchy–Schwarz inequality are used to reduce the computational complexity in the encoding phase [23]–[25]. In the diagnostic phase, the concept of Cauchy–Schwarz inequality is employed to develop an adaptive threshold criterion to detect abnormal regions of the BUT. The proposed VQ-based comparison technique (VBCT) is summarized as follows.

1) Codebook Generation: In this phase, the gold thermal image is divided into N blocks denoted as $\boldsymbol{z}_j$ containing L pixels. Let blocks $\{\boldsymbol{z}_j\}$ be the input to the CFHNN to generate a codebook with C codewords $\{\boldsymbol{w}_i\}$ as described in Section II-A and shown in Fig. 2. The CFHNN algorithm is described in detail as follows.

- Step 1) Input a set of training samples $\boldsymbol{Z} = \{\boldsymbol{z}_1, \boldsymbol{z}_2, \ldots, \boldsymbol{z}_N\}$ with the given number of codewords C, fuzzification parameter $m = 1.2$, constant $\nu = 1$ (these values are selected according to [22]), set the convergence threshold $\varepsilon = 0.005$, and initialize the membership functions of jth training samples for all neurons $\boldsymbol{U}_j = \{\mu_{1,j}, \mu_{2,j}, \ldots, \mu_{C,j}\}$, where $j = 1, 2, \ldots, N$ and $1 = \sum_{i=1}^{C} \mu_{i,j}$. Then, set $j = 1$.
- Step 2) Compute the input bias $I_{i,j} = \nu \tanh(\alpha_i)$, where α_i is defined in (7).
- Step 3) Compute the interconnecting weight vector $\boldsymbol{W}_{i,j;i,k}$ using (6).
- Step 4) Calculate the input $Net_{i,j}$ for each neuron (i,j).
- Step 5) Apply (8) to update the membership values for all the neurons
- Step 6) Increase j by one. If $j \leq N$, then go to step 2; otherwise, set $j = 1$ and then go to step 7.
- Step 7) Update $U^{t+1} = \{\boldsymbol{U}_1, \boldsymbol{U}_2, \ldots \boldsymbol{U}_N\}$ and then compute $\Delta = \max(|\boldsymbol{U}^{t+1} - \boldsymbol{U}^t|)$. If $\Delta > \varepsilon$, then go to step 2; otherwise, go to step 8.
- Step 8) Find all codewords $\boldsymbol{w}_i$ using (9)

2) Encoding Phase: After the codebook for gold thermal image is generated, the index can be found as the least square Euclidean distance between codeword $\boldsymbol{w}_i$ and input vector $\boldsymbol{z}_j$. Mapping $Q(\boldsymbol{z}_j) = \boldsymbol{w}_i$ that assigns an index i to each block $\boldsymbol{z}_j$ must satisfy

$$SED_{i,j} = \min_{i \in p} \left\{ d^2(\boldsymbol{w}_p, \boldsymbol{z}_j) \right\} \quad for\ p = 1, 2, \ldots, C \quad (10)$$

where

$$d^2(\boldsymbol{w}_p, \boldsymbol{z}_j) = \sum_{s=1}^{L} (w_{p,s} - z_{j,s})^2, \tag{11}$$

$$\boldsymbol{w}_p = \{w_{p,s}, s = 1, 2, \ldots, L\} \tag{12}$$

and

$$\boldsymbol{z}_j = \{z_{j,s}, s = 1, 2, \ldots, L\}. \tag{13}$$

The mean value of each block in gold thermal image and a codeword in codebook is used for fault diagnosis. The relation between the Euclidean distance $SED_{i,j}$ and the mean distance between $\boldsymbol{z}_j$ and $\boldsymbol{w}_i$ will be described in the following section.

3) Euclidean Distance Measure: First, we define the squared distance between the sum of components of a block in gold thermal image and a codeword as

$$SMD_{i,j} = \left(\sum_{s=1}^{L} w_{i,s} - \sum_{s=1}^{L} z_{j,s} \right)^2. \tag{14}$$

Moreover, the mean values of $\boldsymbol{z}_j$ and $\boldsymbol{w}_i$ are, respectively, computed as

$$m_j = \frac{1}{L} \sum_{s=1}^{L} z_{j,s} \tag{15}$$

and

$$m_i = \frac{1}{L} \sum_{s=1}^{L} w_{i,s}. \tag{16}$$

According to (10), $SED_{i,j}$ can be described as $SED_{i,j} = \sum_{s=1}^{L} (w_{i,s} - z_{j,s})^2$. Hence, according to the Cauchy–Schwarz inequality [26], $|a_1 b_1 + a_2 b_2 + \cdots + a_L b_L|^2 \leq (|a_1|^2 + |a_2|^2 + \cdots + |a_L|^2) \times (|b_1|^2 + |b_2|^2 + \cdots + |b_L|^2)$. For $a_1 = a_2 = \cdots = a_L = 1$ and $b_s = w_{i,s} - z_{j,s}$, the relation between $SED_{i,j}$ and $SMD_{i,j}$ should satisfy the following condition

$$SMD_{i,j} \leq L \cdot SED_{i,j}. \tag{17}$$

Then, substituting (15) and (16) to (14), $SMD_{i,j}$ can be represented as $SMD_{i,j} = L^2 (m_i - m_j)^2$. The difference between m_i and m_j, and the Euclidean distance $SED_{i,j}$ between $\boldsymbol{w}_i$ and $\boldsymbol{z}_j$ will, thus, satisfy the inequality as (17) and can be further simplified as

$$|m_i - m_j| \leq \frac{ED_{i,j}}{\sqrt{L}} \tag{18}$$

where

$$ED_{i,j} = \sqrt{\sum_{s=1}^{L} (w_{i,s} - z_{j,s})^2}. \tag{19}$$

Since the Euclidean distance between $\boldsymbol{z}_j$ and $\boldsymbol{w}_i$ is minimized, the mean temperature of $\boldsymbol{z}_j$ can be represented by the mean temperature of $\boldsymbol{w}_i$, and the error of mean temperature will be limited by (18). Due to the fact that the gray level of a pixel in the gold thermal image having the maximal operating temperature in the same position for all good boards, the mean temperature of block $\boldsymbol{z}_j$ in gold thermal image would be greater than the mean temperature of block $\boldsymbol{z}_k$ in the thermal image of the BUT.

If m_k is the mean temperature in a proper block of the BUT, then it is true that $m_k \leq m_j$ and it should also satisfy the following equation

$$|m_i - m_k| \leq \frac{ED_{i,j}}{\sqrt{L}}. \tag{20}$$

As mentioned previously, vector quantization is a technique that maps training vectors $\boldsymbol{Z} = \{\boldsymbol{z}_j, j = 1, 2, \ldots, N\}$ in Euclidean $l \times l$-dimensional space $R^{l \times l}$ into a set of $\boldsymbol{W} = \{\boldsymbol{w}_i, i = 1, 2, \ldots, C\}$ points in $R^{l \times l}$, called a codebook. The mapping is usually defined to minimize expected distortion measure $E[d(\boldsymbol{w}_i - \boldsymbol{z}_j)]$ using the mean square error (MSE) given by $d(\boldsymbol{w}_i, \boldsymbol{z}_j) = (\boldsymbol{w}_i - \boldsymbol{z}_j)^T (\boldsymbol{w}_i - \boldsymbol{z}_j)$. Fig. 4(b) shows the image reconstructed from the codebook designed by the CFHNN algorithm with codebook size $C = 64$ and codeword size $L = 4 \times 4$. It produces a high PSNR(38.8 dB) for this image. Note that PSNR is 27.76 dB for the test image Lenna reconstructed from the codebook designed by CFHNN with $C = 64$ and $L = 4 \times 4$. According to the CFHNN algorithm, codeword $\boldsymbol{w}_i$ contains the intensity variation of all the associated blocks $\{\boldsymbol{z}_j\}$. With (18), m_k in normally functioning BUT will be limited to the range between the upper mean temperature m_U and the lower mean temperature m_L

$$m_U = m_i + \frac{ED_{i,j}}{\sqrt{L}} \tag{21}$$

and

$$m_L = m_i - \frac{ED_{i,j}}{\sqrt{L}}. \tag{22}$$

When the mean (m_k) of the block $\boldsymbol{z}_k$ is compared with the mean (m_i) of the associated codeword $\boldsymbol{w}_i$, then the block $\boldsymbol{z}_k$ is identified as a faulty block, if $|m_k - m_i| > |m_j - m_i|$. Furthermore, if m_k and m_i satisfy (20), then according to the (10), codeword $\boldsymbol{w}_i$ is assigned to the block $\boldsymbol{z}_k$. This is a normally functioning block as described above.

Consequently, (21) is used to assure that the mean temperature m_k of the block $\boldsymbol{z}_k$ is mapped to the same codeword $\boldsymbol{w}_i$, as well as block $\boldsymbol{z}_j$. If m_k is greater than m_U, it implies that the mean temperature of the block $\boldsymbol{z}_k$ is greater than that of the block $\boldsymbol{z}_j$. It can be easily seen that the block $\boldsymbol{z}_k$ in the BUT is a faulty block.

4) Diagnostic Phase: The thermal image of the BUT is also divided into N blocks, and each block $\boldsymbol{z}_k$ consists of L pixels (i.e., $\boldsymbol{w}_i$, $\boldsymbol{z}_j$, and $\boldsymbol{z}_k$ are of equal size). However, the thermal information about the gold thermal image is blended into a codebook. Accordingly, in the diagnostic phase the mean difference between $\boldsymbol{z}_k$ and its corresponding codevector $\boldsymbol{w}_i$ is computed instead of the thermal subimage of the specific region [9], device [1], [10], or hot spots [6], [12], [13] in the conventional methods.

5) Adaptive Threshold Criterion: Before comparing each block $\boldsymbol{z}_k$ in the BUT with each codeword $\boldsymbol{w}_i$, not only the index i for the block $\boldsymbol{z}_j$ (in the gold thermal image) that is calculated

from (10) but also the Euclidean distance $ED_{i,j}$ between each block $\boldsymbol{z}_j$ and codeword $\boldsymbol{w}_i$ that is generated in the encoding phase are saved. Furthermore, the codewords are sorted by their mean values in ascending order. Thus, when the mean temperature m_k is greater than m_U, it will be evident in the diagnostic phase that block $\boldsymbol{z}_k$ (in the thermal image of BUT) is not represented by the codeword $\boldsymbol{w}_i$. In other words, the mean temperature of block $\boldsymbol{z}_k$ in the BUT is greater than that of the corresponding block $\boldsymbol{z}_j$ in gold thermal image. This block $\boldsymbol{z}_k$ will be identified as a faulty block.

However, the greater the Euclidean distance $ED_{i,j}$, the smaller the sensitivity of the fault detection. For further explanation, let us define

$$\Delta_{i,j} = \frac{ED_{i,j}}{\sqrt{L}} \tag{23}$$

$$DM_i = m_{i+1} - m_i \tag{24}$$

where $\Delta_{i,j}$ represents the maximum distance between the block $\boldsymbol{z}_j$ and codeword $\boldsymbol{w}_i$, and DM_i is the distance of mean values of the adjacent codewords. In particular, if $\Delta_{i,j}$ is greater than DM_i, according to (21) m_U will then be greater than m_{i+1}. In this case, although m_k (the mean value of the associated block $\boldsymbol{z}_k$ in the BUT) satisfying (20), m_k may be greater than m_{i+1} in application.

In order to increase the diagnostic sensitivity, we have proposed an adaptive threshold technique when the value of $\Delta_{i,j}$ is too large. Accordingly, this criterion technique will be applied to classify block $\boldsymbol{z}_k$ as a faulty block if the following criteria are met.

Criterion 1) $m_k > m_U$ *and* $\Delta_{i,j} \leq DM_i$.
Criterion 2) $m_k > m_{i+1}$ *and* $\Delta_{i,j} > DM_i$.

Criterion 1) means that the mean value m_k of the block $\boldsymbol{z}_k$ does not satisfy (20). It implies that block $\boldsymbol{z}_k$ does not belong to codeword $\boldsymbol{w}_i$ in general case. In other words, the distance between $\boldsymbol{z}_k$ and $\boldsymbol{w}_i$ is greater than the distance between $\boldsymbol{z}_j$ and $\boldsymbol{w}_i$. Certainly, the block $\boldsymbol{z}_k$ in the BUT is a faulty block.

Criterion 2) applies to the case when the Euclidean distance between $\boldsymbol{z}_j$ and $\boldsymbol{w}_i$ is too large such that there exists practically a large mean temperature error for the block $\boldsymbol{z}_j$ being represented by the codeword $\boldsymbol{w}_i$. To solve this problem, we apply Criterion 2) to reduce the threshold value. In summary, when the mean value of the block $\boldsymbol{z}_k$ in the BUT satisfies (20), we still classify this block as a faulty block, if Criterion 2) is met.

The detailed description of the proposed method to detect faulty block is summarized in the following.

Step 1) Divide the gold thermal image of PCB into N blocks ($\boldsymbol{z}_j$ represents the j's block) with L elements.
Step 2) Use the CFHNN to design the codebook.
Step 3) Apply (10) to search each block $\boldsymbol{z}_j$ mapping to the ith codeword in the codebook and record $\Delta_{i,j}$ which is defined in (23). In addition, record the mean value m_i for each codeword $\boldsymbol{w}_i$, and store the distance about the mean value between each adjacent codeword DM_i presented in (24) and the upper limit mean value m_U as described in (21).

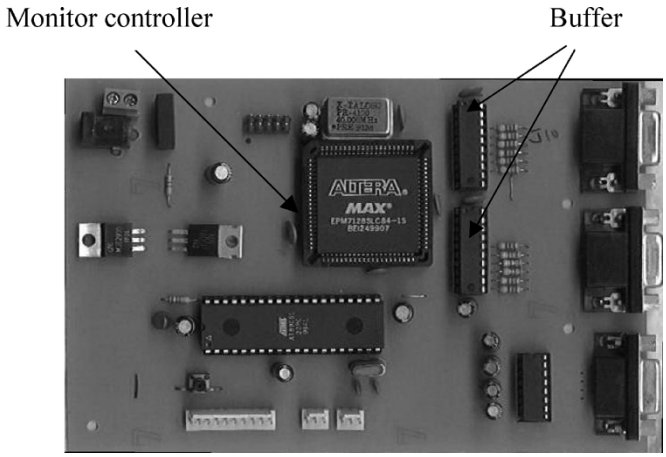

Fig. 3. Picture of the monitor control board.

Step 4) Divide the thermal image of the BUT into N blocks. The size of the block is the same as the block $\boldsymbol{z}_j$ and the codeword $\boldsymbol{w}_i$.
Step 5) Detect the faulty block, using the adaptive threshold criterion technique.

III. Application Examples

In this experiment, monitor control board as shown in Fig. 3 (this board controls the DTK C505 monitor working in 800 $\times$ 600 pixels resolution) was investigated using the proposed method. Five thermal images for five boards with functional clock were acquired using the Agema Thermovision 550 SW thermal camera to extract a gold thermal image. The thermal images for the boards with abnormal functional clocks or floating pins were obtained for fault diagnosis. The image size is 320 by 240. Some parameters of this system are summarized as follows. The thermal sensitivity is 0.1 °C at 30 °C, the wavelength range for infrared PtSi detector is 3.6–5.0 μm, the field of view is 20° $\times$ 15°, and the minimal focal distance is 40 cm.

The distance between the camera and the BUT was set to 70 cm. In order to reduce the noise effect of the ambient temperature, the BUT was placed in a chamber. The inner surface of this chamber was painted black to reduce thermal reflection. According to the investigation of Allred *et al.* [6], an IC chip would be still in an adiabatic state at the first 50 seconds after power on. Thus, in order to avoid thermal stagnation, the thermal image for the BUT was captured at the 40th second after power on.

Two major components, an Altera CPLD chip (EPM7128SLC84) and its two buffer chips of this BUT, are the target area for diagnosis. Since the power consumption of these chips is proportional to the running clock frequency, a board with 40-MHz clock is considered to be in normal state, and boards with 50 and 80 MHz are considered in abnormal and denoted as BUT1 and BUT2, respectively. Moreover, the thermal distribution will highly depend on the power pin connection of the chip. Thus, the boards of two or three floating power pins were used as faulty boards denoted as BUT3 and BUT4, respectively. The gold thermal image containing these three chips is shown in Fig. 4(a). The gold thermal image reconstructed from the codebook is shown in

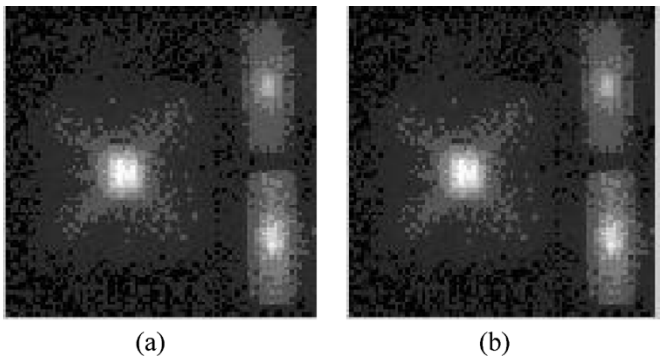

Fig. 4. (a) The gold thermal image extracted from five faultless boards. (b) Gold thermal image reconstructed from the codebook.

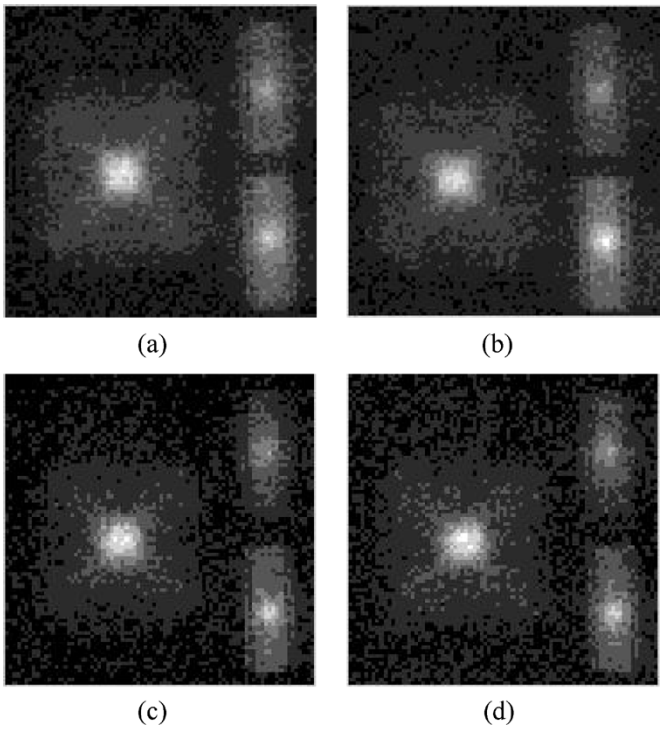

Fig. 5. Thermal images of monitor control board with some fault. (a) BUT1 is the board working at 50 MHz. (b) BUT2 working at 80 MHz. (c) BUT3 is the monitor controller with two power pins floating. (d) BUT4 with three power pins floating.

Fig. 4(b). The abnormal thermal images corresponding to various fault modes are displayed in Fig. 5.

Obviously, it is very difficult to tell the difference between Figs. 4 and 5 with only visual inspection. This proposed method with the adaptive threshold criteria is referred to as vector-based comparison technique (VBCT) and applied to fault diagnosis. Each mean value of the block between BUT and the mapping codeword is computed and compared. On the contrary, the method that directly uses the mean values of both corresponding blocks in the gold thermal image and the BUT for fault diagnosis is called the block-based comparison technique (BBCT). For the performance comparison, the BBCT is also applied.

Figs. 6–9 show the experimental results including BUT working at 50 and 80 MHz, with two power pins floating, and three power pins floating, respectively. (a) and (b) in Figs. 6–9 show the identified faults using BBCT and VBCT methods, respectively. There are only two blocks that were misclassified in BUT1 by the VBCT method. The recognition rate is 99.5%.

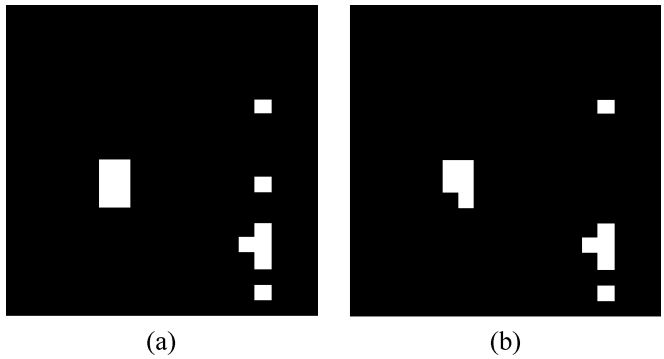

Fig. 6. Identified fault regions for BUT1 using (a) BBCT and (b) VBCT.

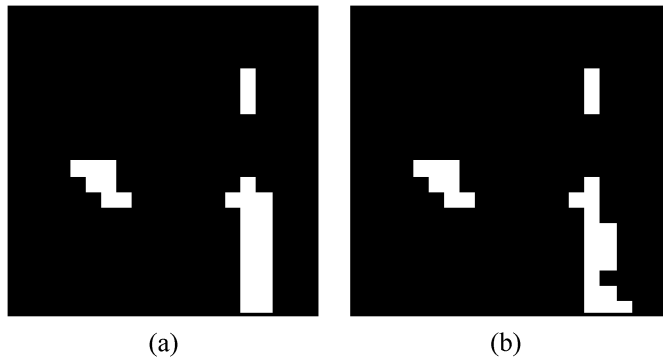

Fig. 7. Identified fault regions for BUT2 using (a) BBCT and (b) VBCT.

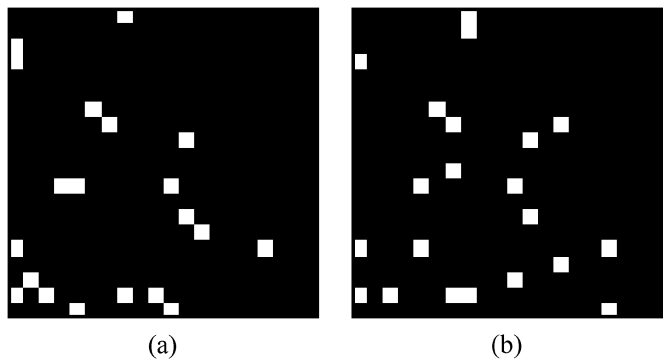

Fig. 8. Identified fault regions for BUT3 using (a) BBCT and (b) VBCT.

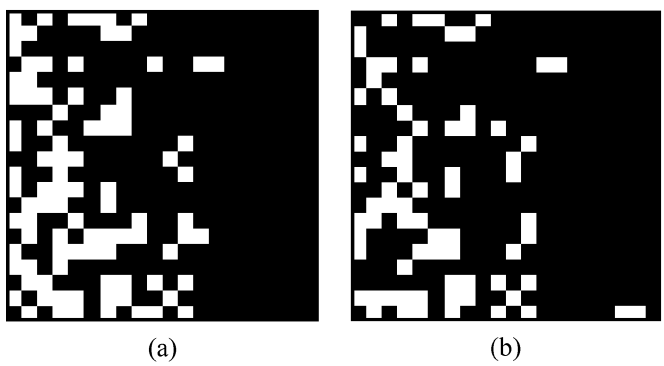

Fig. 9. Identified fault regions for BUT4 using (a) BBCT and (b) VBCT.

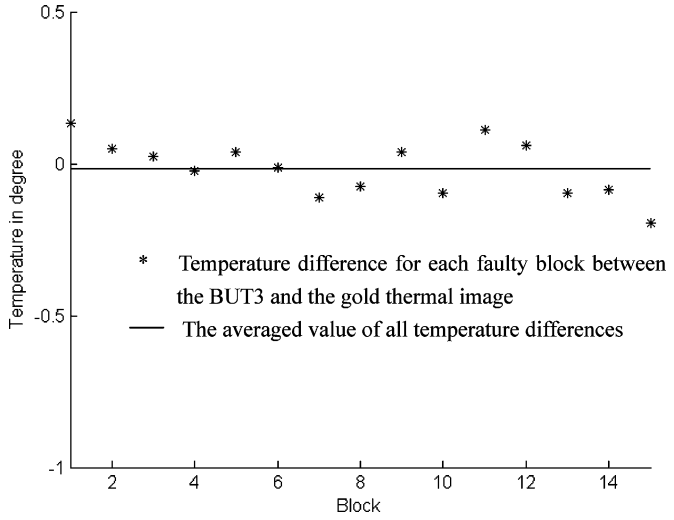

Fig. 10. Temperature differences and averaged temperature difference for each faulty block between the BUT3 and the gold thermal image in VBCT method.

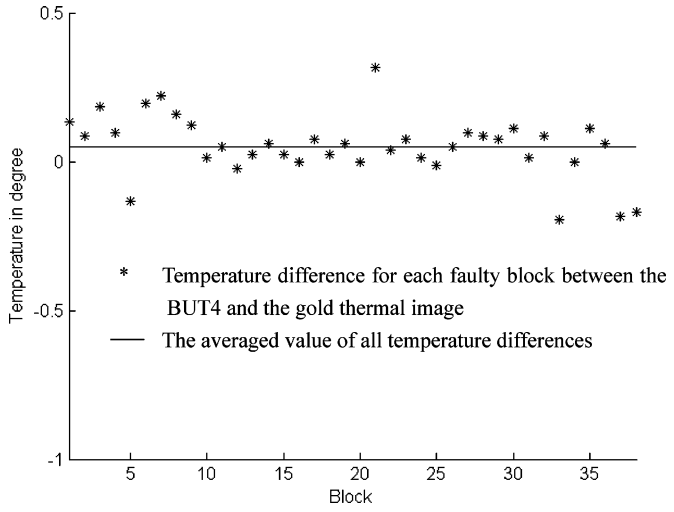

Fig. 11. Temperature differences and averaged temperature difference for each faulty block between the BUT4 and the gold thermal image in VBCT method.

For BUT2, BUT3, and BUT4, the recognition rates are 99%, 96.25%, and 90.5%, respectively. Furthermore, Figs. 10 and 11 show the temperature differences in each faulty block between BUT3 and gold image, and BUT4 and gold image. The values of mean and standard deviation are −0.016 °C and 0.089 °C for Fig. 10, and 0.051 °C and 0.103 °C for Fig. 11. From the experimental results, it is shown that the proposed VQ-based diagnostic system is very effective in PCB inspection.

IV. Concluding Remarks

In this paper, a novel system based on thermal image analysis for printed circuit board diagnosis is presented. It is based on the codeword generated from the gold thermal image. The proposed VQ-based approach for the PCB inspection can reduce the memory size in storing the gold thermal image. In addition, by the introduction of adaptive threshold criteria, each codeword may be compared with its actual associated block in the BUT. The experimental results indicate that up to 90.5% of faulty blocks can be identified using the proposed method. Since the proposed method is based on the Hopfield neural network, it is highly modularized and may be parallelized for speeding up the processing to run on a multiprocessor system or in a pipelined architecture. Besides, only the mean computation and comparison are involved in this approach; the diagnostic phase of our system can easily be implemented in hardware. The disadvantage of this system is that the mean values of the codewords are nonlinearly distributed over the whole codebook, especially for the mean values of two adjacent codewords being too close or similar. This problem will be further investigated in future study.

Acknowledgment

The authors would like to thank Prof. Herchang Ay at the Department of Mechanical Engineering, Southern Taiwan University of Technology, Tainan, Taiwan, R.O.C., and the colleagues from the Image Processing Lab, Department of Electronic Engineering, National Chin-Yi Institute of Technology, Taichung, Taiwan, for their valuable comments.

References

[1] H. F. Spence and D. P. Burris, "An artificial neural network printed circuit board diagnostic system based on infrared energy emissions," in *Proc. IEEE Systems Readiness Technology Conf.*, Anaheim, CA, Sep. 24–26, 1991, pp. 41–45.

[2] A. Poitier and W. J. Marusa, Jr., "Image processing, a new diagnostic tool," *IEEE Aerospace and Electronics Systems Mag.*, vol. 9, no. 3, pp. 34–37, Mar. 1994.

[3] S. C. Yao and K. E. Su, "Thermal analysis of a two-dimensional electronic board," in *Proc. I—THERM*, Los Angeles, CA, May 11–13, 1988, pp. 79–84.

[4] S. Witzman, D. Newport, and T. Nicoletta, "Free convection air cooling of the electronic equipment: Still a miracle waiting to be explored and explained," in *Proc. 5th Annu. IEEE SEMI-THERM V.*, San Diego, CA, Feb. 7–9, 1989, pp. 98–103.

[5] W. M. Foster, "Thermal verification testing of commercial printed-circuit boards for spaceflight," in *Proc. Ann. Reliability and Maintainability Symp.*, Las Vegas, NE, Jan. 1992, pp. 189–195.

[6] L. G. Allred and G. E. Kelly, "A system for fault diagnosis in electronic circuits using thermal imaging," in *Proc. IEEE Systems Readiness Technology Conf.*, Dayton, OH, Sep. 1992, pp. 455–458.

[7] B. Linnander, "When it's too hot to touch use infrared thermography," *IEEE Circuits and Devices Mag.*, vol. 9, no. 4, pp. 35–37, Jul. 1993.

[8] D.-H. Lee, "Thermal analysis of integrated-circuit chips using thermographic imaging techniques," *IEEE Trans. Instrum. Meas.*, vol. 43, no. 6, pp. 824–829, Dec. 1994.

[9] S. A. Merryman and R. M. Nelms, "Diagnostic technique for power systems utilizing infrared thermal imaging," *IEEE Trans. Ind. Electron.*, vol. 42, no. 6, pp. 615–628, Dec. 1995.

[10] D. Washburn and M. Nguyen, "Commercial off the shelf (COTS)/non developmental item (NDI) testing for department of defense using infra-red technology," in *Proc. Autotestcon Systems Readiness: Test Technology 21st Century*, Atlanta, GA, Aug. 1995, pp. 584–587.

[11] K. Azar and J. E. Graebner, "Experimental determination of thermal conductivity of printed wiring boards," in *Proc. 12th Annu. IEEE SEMI-THERM XII*, Austin, TX, Mar. 1996, pp. 169–182.

[12] L. G. Allred and T. R. Howard, "Thermal imaging is the sole basis for repairing circuit cards in the F-16 flight control panel," in *Proc. Autotestcon Test Technology Commercialization*, Dayton, OH, Sep. 1996, pp. 418–424.

[13] L. G. Allred and J. P. Harames, "Guidelines for successful implementation of infrared thermography for repairing electronic circuit cards," in *Proc. Autotestcon, Test Technology Commercialization*, Dayton, OH, Sep. 1996, pp. 410–417.

[14] P. J. Moore and F. Harscoet, "Low cost thermal imaging for power systems applications using a conventional CCD camera," in *Proc. EMPD*, vol. 2, Singapore, Mar. 1998, pp. 589–594.

[15] L. G. Allred, "Using infrared thermography to detect age degradation in EPROM chips," in *Proc. Autotestcon Systems Readiness Technology Conf.*, Salt Lake City, UT, Aug. 1998, pp. 546–551.

[16] F. P. Incropera and D. P. DeWitt, *Fundamentals of Heat Transfer*. New York: Wiley, 1981.
[17] X. P. V. Maldague, *Infrared Methodology and Technology*. New York: Gordon and Breach, 1994.
[18] R. M. Gray, "Vector quantization," *IEEE Signal Process. Mag.*, vol. ASSP-1, pp. 4–29, Apr. 1984.
[19] Y. Linde, A. Buzo, and R. M. Gray, "An algorithm for vector quantizer design," *IEEE Trans. Commun.*, vol. COM-28, pp. 85–94, Jan. 1980.
[20] A. Gersho and R. M. Gray, *Vector Quantization and Signal Compression*. Norwell, MA: Kluwer, 1992.
[21] J.-S. Lin, S.-H. Liu, and C.-Y. Lin, "The application of fuzzy Hopfield neural network to design better codebook for image vector quantization," *IEICE Trans. Fundamentals*, vol. E81-A, no. 8, pp. 1645–1651, 1998.
[22] S.-H. Liu and J.-S. Lin, "A compensated fuzzy Hopfield neural network for codebook design in vector quantization," *Int. J. Patt. Recog. Artif. Intell.*, vol. 14, no. 8, pp. 1067–1079, Dec. 2000.
[23] S. W. Ra and J. K. Kim, "A fast mean-distance-ordered partial codebook search algorithm for image vector quantization," *IEEE Trans. Circuits Syst. II: Analog Digit. Signal Process.*, vol. 40, no. 9, pp. 576–579, Sep. 1993.
[24] C. H. Lee and L. H. Chen, "Fast closest codeword search algorithm for vector quantization," *IEE Proc.—Vision, Image and Signal Process*, vol. 141, no. 3, pp. 143–148, Jun. 1994.
[25] S. J. Baek, B. K. Jeon, and K.-M. Sung, "A fast encoding algorithm for vector quantization," *IEEE Signal Process. Lett.*, vol. 4, no. 12, pp. 325–327, Dec. 1997.
[26] M. R. Spiegel, *Mathematical Handbook of Formulas and Tables*. New York: McGraw-Hill, 1968.

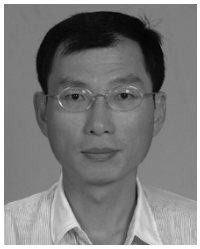

Shih-Yuan Huang was born in Taiwan in 1961. He received the M.S. degree in electrical engineering from National Taiwan University, Taipei, Taiwan, R.O.C., in 1987. He is currently working towards the Ph.D. degree in electrical engineering at National Cheng Kung University, Tainan, Taiwan.

Since 1991, he has been an Instructor with the Department of Electronic Engineering, National Chin-Yi Institute of Technology, Chungli, Taiwan. His research interests include digital image processing and digital circuit design.

Chi-Wu Mao was born in Taiwan in 1939. He received the B.S. degree in electrical engineering from the National Cheng Kung University, Tainan, Taiwan, R.O.C., in 1963 and the M.S. degree from Purdue University, West Lafayette, IN, in 1970.

Since 1970, he has been with the Department of Electrical Engineering, National Cheng Kung University, where he is now a Professor. His research interests are human hidden energy engineering, electrical magnetic and digital image processing.

Kuo-Sheng Cheng (M'91–SM'98) was born in Taipei, Taiwan, R.O.C. He received the B.S., M.S., and Ph.D. degrees in electrical engineering from the National Cheng Kung University, Tainan, Taiwan. He also received the M.S. degree in biomedical engineering from the Rensselaer Polytechnic Institute, Troy, NY, in 1988.

Since 1989, he has been with the Institute of Biomedical Engineering, National Cheng Kung University. Currently, he is a Professor and President of the Biomedical Engineering Society of the Taiwan. His research interests are bioimpedance imaging, bioelectronics, and medical image processing.